Journal of Hydroscience and Hydraulic Engineering
Vol. 17, No.1 May, 1999, 103-116

# 3D NUMERICAL PREDICTION METHOD FOR LOCAL SCOUR DUE TO BUOYANT JETS IN NEARSHORE FIELD

By

Satoru Ushijima, Takao Shimizu and Minoru Hosaka*

Central Research Institute of Electric Power Industry (CRIEPI)
1646 Abiko, Abiko-shi, Chiba-ken, 270-1194, Japan

*Tohoku Electric Power Co., Inc., Research and Developing Center
7-2-1 Nakayama Aoba-ku, Sendai-shi, Miyagi-ken, 981, Japan

## SYNOPSIS

A numerical prediction method is developed for sand bed deformation due to horizontally discharged buoyant jets. Three-dimensional buoyant flows and sediment transportation are predicted with a two-equation turbulence model. In order to represent unsteadily deformed bed profiles, three-dimensional boundary-fitted coordinates are regenerated at regular intervals and the moving boundaries are treated on the basis of the arbitrary Lagrangian-Eulerian (ALE) formulation. The governing equations are transformed into a mapped space and discretized on a Lagrangian scheme with third-order accuracy for advection terms. This computational method is applied to a nearshore area where local scour is caused by cooling-water discharge. The sand bed profiles actually measured in the field are compared with the predicted results.

## INTRODUCTION

The accurate estimation for sediment transportation and resulting bed deformation is essential to design hydraulic structures exposed to these phenomena and to assess their long-term stability.

In nearshore regions, local scour may arise on a sand bed in front of a power station when cooling water is discharged with high velocity from its submerged outlets. In this problem, it is necessary to deal with turbulent flows affected by buoyancy force above the unsteadily deformed bottom boundaries. Therefore, most of the empirical formulations, which were usually derived in fairly simple hydraulic conditions, are no longer available. In addition, although many numerical techniques have been proposed so far, it is obvious that we cannot obtain any useful information from two-dimensional or quasi-three-dimensional models.

A desired approach is to employ a complete three-dimensional numerical method with adequate treatment for the unsteadily and non-uniformly deformed boundaries. Three-dimensional numerical methods for local scour were proposed in the past by Ushijima et al. (1), Olsen and Melaaen (2), Ushijima (3) and others. In these methods, however, only an isothermal flow field can be dealt with and they were verified using only experimental results obtained in the laboratory. Thus, it is necessary to extend the applicability of usual techniques to more general conditions and to verify them with the data actually measured in a field.

In the present study, a numerical prediction method is developed for bed deformation due to three-dimensional turbulent flows affected by buoyancy force. In this method, the buoyant flows and sediment transportation are predicted with a two-equation turbulence model. The effects of the unsteadily deformed bed profiles on a flow field are adequately taken into account, since the boundary shapes are precisely represented using three-dimensional boundary-fitted coordinates (4), which are generated repeatedly to respond to unsteady deformation. In this coordinate system, the moving boundary is

treated with the arbitrary Lagrangian-Eulerian (ALE) formulation (5) and the governing equations are transformed into a mapped space, where discretization is made with sufficient numerical accuracy.

This computational method is applied to a nearshore region where sand bed is scoured by cooling-water discharge from a power station. The bed profiles actually measured in the field are compared with the predicted results. From the comparison, it will be shown that the applicability of the present numerical method to actual fields is satisfactory. The derived computational method is expected to be applied to wide range of sediment transportation and bed-deformation problems in hydraulics, in terms of the accuracy and the generality of the present numerical model and solution algorithm.

## NUMERICAL PROCEDURE

### *Grid Generation*

The sand bed profiles unsteadily deformed by flows can be treated as moving boundaries. Thus, three dimensional boundary-fitted coordinates are employed to represent complicated-shaped bed profiles and the coordinates are regenerated at regular intervals in order to respond precisely to the unsteady deformation. The movements of computational grid points, arising from this approach for moving boundaries, are adequately taken into account in the governing equations on the basis of the ALE formulation.

Let $(t, x_i)$ and $(\tau, \xi_m)$ be the time and three-dimensional spatial coordinates in the physical and mapped (or computational) spaces, respectively $(i, m = 1, 2, 3)$. The present boundary-fitted coordinates can be obtained from the following equation (4):

$$\left(\frac{\partial^2 x_i}{\partial \xi_p \partial \xi_q}\right)^* \left(\frac{\partial \xi_p}{\partial x_j}\right)^* \left(\frac{\partial \xi_q}{\partial x_j}\right)^* + \frac{\partial^2 x_i}{\partial \xi_r \partial \xi_s} \left(\frac{\partial \xi_r}{\partial x_j}\right)^* \left(\frac{\partial \xi_s}{\partial x_j}\right)^* + P_m \left(\frac{\partial x_i}{\partial \xi_m}\right)^* = 0 \tag{1}$$

where $p \neq q$ and $r = s$. The Einstein summation rule is applied to the terms bearing the same subscripts twice in this paper. The control functions $P_m$ may be used to arrange the grid intervals in the physical space. In Eq. 1, the derivatives having asterisks are not evaluated by the usual central difference, but from the general cubic spline interpolation (GCSI) as proposed by Ushijima (6) to improve the numerical accuracy in grid generation.

### *Governing Equations For Turbulent Buoyant Flows*

The equations of motion are Reynolds equations, derived as the ensemble-averaged Navier-Stokes equations. When using a general $k - \epsilon$ model, the Reynolds equations may be given as the following forms in the physical space:

$$\frac{Du_i}{Dt} = -\frac{1}{\rho}\frac{\partial p}{\partial x_i} + (1 - \beta \Delta T)\, g_i + \frac{\partial}{\partial x_j}\left[(\nu + \epsilon_M)\left(\frac{\partial u_i}{\partial x_j} + \frac{\partial u_j}{\partial x_i}\right)\right] - \frac{3}{2}\frac{\partial k}{\partial x_i} \tag{2}$$

Here $u_i$, $g_i$, $p$, $\rho$, $\beta$, $\Delta T$, $\epsilon_M$ and $\nu$ are average velocity and gravity acceleration in $x_i$ direction, pressure, fluid density, thermal expansion coefficient, temperature difference from a standard value, and eddy and kinematic viscosities, respectively. The momentum equations are transformed into the computational space and then discretized as described later.

The energy equation in the physical space is given by

$$\frac{DT}{Dt} = \frac{\partial}{\partial x_j}\left[(\alpha + \epsilon_H)\frac{\partial T}{\partial x_j}\right] \tag{3}$$

where $T$, $\epsilon_H$ and $\alpha$ are average temperature, eddy and molecular conductivities respectively. The eddy conductivity may be given with the eddy diffusivity and turbulent Prandtl number $P_{rt}$:

$$\epsilon_H = \frac{\epsilon_M}{P_{rt}} \tag{4}$$

Since the turbulent Prandtl number is affected by the vertical temperature distribution, it is modeled as the following form proposed by Ushijima et al. (7):

$$\frac{1}{P_{rt}} = \frac{1.6}{1+0.24B_L} \tag{5}$$

where the buoyancy parameter $B_L$, proposed by Launder (8), is defined by

$$B_L = \beta g \left(\frac{k}{\epsilon}\right)^2 \frac{\partial T}{\partial x_3} \tag{6}$$

with the vertically-upward coordinate $x_3$.

The transport equations for turbulence energy $k$ and its dissipation rate $\epsilon$ are written in the physical space as

$$\begin{aligned}\frac{Dk}{Dt} &= \epsilon_M \left(\frac{\partial u_i}{\partial x_j} + \frac{\partial u_j}{\partial x_i}\right)\frac{\partial u_i}{\partial x_j} - \beta g \epsilon_H \frac{\partial T}{\partial x_3} \\ &+ \frac{\partial}{\partial x_j}\left[\left(\nu + \frac{C_k}{C_\nu}\epsilon_M\right)\frac{\partial k}{\partial x_j}\right] - \epsilon\end{aligned} \tag{7}$$

and

$$\begin{aligned}\frac{D\epsilon}{Dt} &= C_{\epsilon 1}\frac{\epsilon}{k}\epsilon_M \left(\frac{\partial u_i}{\partial x_j} + \frac{\partial u_j}{\partial x_i}\right)\frac{\partial u_i}{\partial x_j} \\ &+ \frac{\partial}{\partial x_j}\left[\left(\nu + \frac{C_\epsilon}{C_\nu}\epsilon_M\right)\frac{\partial \epsilon}{\partial x_j}\right] - C_{\epsilon 2}\frac{\epsilon^2}{k}\end{aligned} \tag{8}$$

The coefficients of the turbulence model are $C_k = C_\nu = 0.09$, $C_\epsilon = 0.075$, $C_{\epsilon 1} = 1.44$, $C_{\epsilon 2} = 1.90$ as proposed by Rodi (9).

Since the ALE formulation is employed, the Lagrangian differential operator, which is defined in the transformed space, is given by

$$\frac{D}{Dt} = \frac{\partial}{\partial \tau} + (U_m - U_{0m})\frac{\partial}{\partial \xi_m} \tag{9}$$

This differential operator is applied to the transformed governing equations. The contravariant velocity components $U_m$ and $U_{0m}$ correspond to the fluid velocity and that of the computational grid point respectively, which are defined as

$$U_m = u_i \frac{\partial \xi_m}{\partial x_i} \tag{10}$$

and

$$U_{0m} = \frac{\partial x_i}{\partial \tau}\frac{\partial \xi_m}{\partial x_i} \tag{11}$$

The transformed governing equations are discretized on a Lagrangian scheme in the computational space. For example, Eq. 2 may be expressed as the following simple form in the transformed space:

$$\frac{Du_i}{Dt} = -PG_i + F_i + D_i \tag{12}$$

where $PG_i$, $F_i$ and $D_i$ stand for the pressure gradient, external force including buoyancy effects and diffusion terms respectively. Taking account of the Taylor expansion for total differentiation up to the second-order terms, Eq. 12 can be discretized in the following form, which was applied to Navier-Stokes equations by Ushijima (6):

$$u_i^{n+1} = u_i'^n + \left[-PG_i^{n+1} + F_i^n + \left(\frac{3}{2}D_i'^n - \frac{1}{2}D_i''^{n-1}\right)\right]\Delta t \tag{13}$$

Here the superscripts stand for the computational step number and prime and double prime mean the values at upstream positions $P'(\xi_1', \xi_2', \xi_3')$ and $P''(\xi_1'', \xi_2'', \xi_3'')$ respectively, where $\xi_m' \equiv \xi_m - (U_m'^n - U_{0m}'^n)\Delta\tau$ and $\xi_m'' \equiv \xi_m - \xi_m' - (U_m'^{n-1} - U_{0m}'^{n-1})\Delta\tau$.

The first term on the right hand side of Eq. 13, corresponding to the convection term, is calculated with the spatial interpolation in which local cubic spline interpolation (LCSI) is utilized in the three-dimensional computational space (6). This evaluation has third-order accuracy and it is effective to decrease numerical diffusion arising from advection terms. It has been shown that the LCSI method is more accurate than third-order upwind scheme even with finer mesh divisions (6).

The other basic equations, energy equation and the transport equations for turbulence quantities, are discretized as Eq. 13. The submodules of our computational method have been applied to the flows in various conditions and verified in detail with their experimental results (1), (7) and (6). Thus, it is expected to have reasonable applicability to the turbulent non-isothermal flows dealt with in the present study.

*Computation of Pressure Field*

Differentiating Eq. 13 with respect to $x_i$, the following equation is derived using a continuity equation for incompressible flows:

$$\frac{\partial^2 p^{n+1}}{\partial\xi_m\partial\xi_n}\left(\frac{\partial\xi_m}{\partial x_j}\right)\left(\frac{\partial\xi_n}{\partial x_j}\right) + P_m\frac{\partial p^{n+1}}{\partial\xi_m} = \frac{\rho}{\Delta t}\left(\frac{\partial U_m'^n}{\partial\xi_m} + \frac{\partial FU_i}{\partial\xi_m}\frac{\partial\xi_m}{\partial x_i}\Delta t\right) \equiv RHS \tag{14}$$

where the continuity equation at $n+1$ computational step is assumed to be satisfied as Harlow and Welch (10). After the spatial discretization of pressure on staggered grid arrangement as done by Ushijima(6), Eq. 14 may be written in the following form:

$$c_0 p_{ijk}^{n+1} + \sum_{m=1}^{21} c_m p_{pqr}^{n+1} = RHS_{ijk} \tag{15}$$

where $p_{pqr}^{n+1}$ is the pressure at the neighboring 21 grid points and $c_m$ means the coefficients independent of the pressure. Eq. 15 reduces to the following matrix equation:

$$\boldsymbol{Ap} = \boldsymbol{b} \tag{16}$$

Here the matrix $\boldsymbol{A}$ consists of $c_m$, and $\boldsymbol{p}$ and $\boldsymbol{b}$ are column vectors formed with $p_{pqr}^{n+1}$ and $RHS_{ijk}$ respectively. This matrix equation is solved with a preconditioned biconjugate gradient method.

## Governing Equations for Sediment Transportation

The continuity equation for bed material is utilized to predict bed profiles. The continuity equation for sands in the physical space is written as

$$(1-\gamma)\frac{\partial B}{\partial t} + \frac{\partial q_i}{\partial x_i} = 0 \tag{17}$$

Here $\gamma$, $B$ and $q_i$ stand for the porosity of bed material, the height of the bed and sediment flux in $x_i$ directions respectively. This equation is also transformed into the computational space and then discretized as other governing equations. The sediment flux may be sum of the bedload and suspended load as treated in our previous work (1), (3). However, most of the empirical bedload equations are derived for equilibrium one-dimensional flows. Thus, as done by Olsen and Melaaen (2), both bedload and suspended load are assumed to be evaluated at the same time with the advection-diffusion equation for sediment concentration. This transport equation is written in the physical space as

$$\frac{D^*C}{Dt} = \frac{\partial}{\partial x_j}\left[(\lambda + \epsilon_S)\frac{\partial C}{\partial x_j}\right] \tag{18}$$

where $C$ is the average sediment concentration and $\epsilon_S$ and $\lambda$ are turbulent and molecular diffusivities for $C$. The Lagrangian differential operator in Eq. 18, defined in the transformed space, includes falling velocity $w_0$ as

$$\frac{D^*}{Dt} = \frac{\partial}{\partial \tau} + \left(U_m - U_{0m} - w_0\delta_{3j}\frac{\partial \xi_m}{\partial x_j}\right)\frac{\partial}{\partial \xi_m} \tag{19}$$

Consequently, the sand flux $q_i$ in Eq. 17 is estimated by vertical integration of the concentration flux, $Cu_i$.

The amount of the lifted sand particles is evaluated by the pick-up rate $p_s$, proposed by Nakagawa and Tsujimoto (11), which is approximated by

$$p_s\sqrt{\frac{d}{(\sigma/\rho - 1)\,g}} = 0.03\tau_*\,(1 - 0.035/\tau_*) \qquad [0.04 < \tau_* < 0.2] \tag{20}$$

where $\sigma$ and $d$ are density and diameter of sand particles. The normalized bottom shear stress $\tau_*$ is defined here as the summation of two components due to discharged flows $\tau_{*f}$ and wave motions $\tau_{*wm}$:

$$\tau_* = \tau_{*f} + \tau_{*wm} \tag{21}$$

The shear stress by the flow is given by

$$\tau_{*f} = \frac{u_{h*}^2}{(\sigma/\rho - 1)\,gd} \tag{22}$$

where the friction velocity $u_{h*}$ is defined by $u_{h*} = (u_{1*}^2 + u_{2*}^2)^{1/2}$ with general logarithmic law for a hydraulically rough wall. The other bottom shear stress caused by wave motions is evaluated by the equation proposed by Jonsson (12) with the assumption of small amplitude waves.

## APPLICATIONS TO FIELD OBSERVATIONS

### *Field Measurements*

In many cases, the verification of numerical methods for bed deformation was made using only experimental results obtained in the laboratory, and field measurements were scarcely reported especially for the scour in front of a power station when cooling water is discharged from its submerged outlets. However, reliable observations have been continued in a thermal power station in northern Japan. In this power station, the topography of the sea bed has been measured every year since 1992 and nearly steady bed profiles are obtained in two different conditions for cooling-water discharge. One result measured in 1995, CASE-A, presents the bed profiles caused by one cooling-water jet from a submerged outlet and the other result in 1996, CASE-B, provides the profiles created by two jets discharged from two outlets.

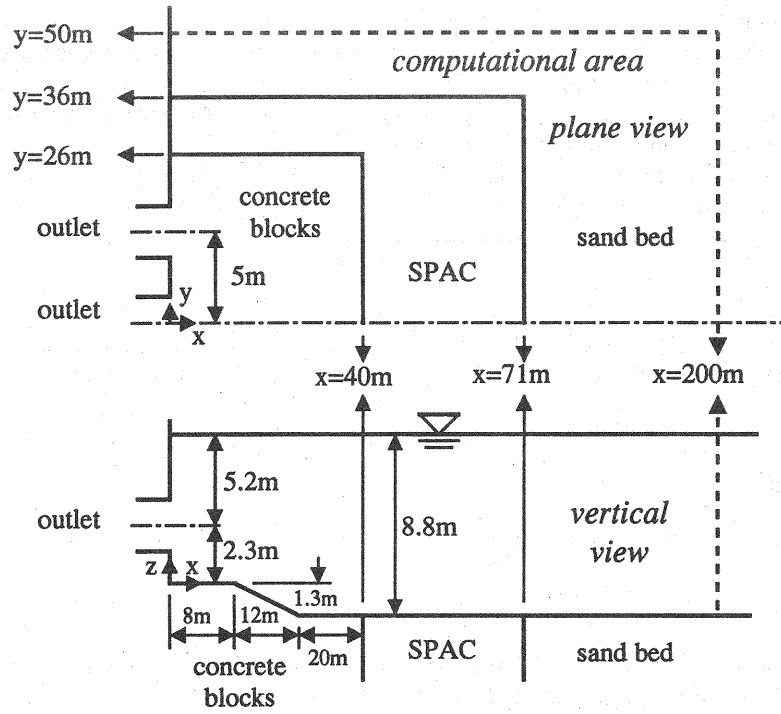


Fig. 1 Schematic view of bed conditions and outlet structures

Fig. 1 shows the schematic view of the bed conditions and outlet structure in the power station. The flow rate of the discharged cooling water is $27.3m^3/s$ per single outlet and its average velocity is nearly $5.0m/s$. As shown in Fig. 1, three submerged outlets are horizontally arranged with equal intervals. The bed area over $x = 0m - 40m$ and $y = 0m - 26m$ is covered with concrete blocks to prevent scour and the bed material over $x = 40m - 71m$ and $y = 26m - 36m$ is replaced with stones about $0.9m$ in diameter, which is called SPAC (Spreading Armor Coat) proposed by Shimizu et al. (13), aiming to protect the upstream concrete block area. The further downstream bed region consists of nearly uniform sand whose diameter is about $0.2mm$, as confirmed by the soil tests.

*Conditions of Computation*

In the present study, the computational method is applied to the results in CASE-A and CASE-B, taking account of the actual plant operation. The conditions for wave motions are determined from the observed data; the time period, wave height and length are $5sec$, $0.7m$ and $35m$, respectively. The discharged cooling water has higher temperature by $7°C$ than that of the environmental water which is assumed to be set at $20°C$. The computational mesh number is $\xi_1 \times \xi_2 \times \xi_3 = 51 \times 35 \times 15 = 26,775$ and each grid point may be referred with indices $i, j$ and $k$, where $i = 1$ (upstream boundary) to $i = 51$, $j = 1$ (symmetrical center boundary) to $j = 35$ (free boundary), and $k = 1$ (bottom boundary) to $k = 15$ (free surface).

Since the effects of wave motions on the bottom boundaries are taken into account as shown in Eq. 21, the free surface is treated as a fixed wall without friction force. The bottom boundary condition for fluid velocity is regulated by a general logarithmic law near a hydraulically rough wall. The symmetric boundary conditions are applied to the vertical section on the center line, while free boundary conditions, in which normal gradients of physical quantities are set at zero, are utilized on the outer boundaries shown by broken lines in Fig. 1.

The computational procedures for local scouring are based on the techniques proposed by Ushijima (3), in which the numerical predictions for turbulent flows and for bed deformation are performed alternately with different computational time increments. This method allows us to deal with the largely

different time scales for these two processes. In the present cases, the time increments in the computations for fluid dynamics and bed deformation are set at $0.25sec$ and $3.6 \times 10^3 sec$ respectively. Since the deformation of sand bed is less than 5 % during the computational process of local scouring, the difference of time increments has no effects on the final sand bed profiles (3). The total computational time for local scour in CASE-A, for example, was about 20 hours using DEC 3000-700 AXP.

*Comparison of the Results*

In the first step of the computation, a steady flow field is obtained assuming the bottom boundary is a fixed surface. Fig. 2 show the distributions of fluid temperature and velocity vectors obtained in this calculation. These results are used as initial conditions for the computation of bed deformation in CASE-A.

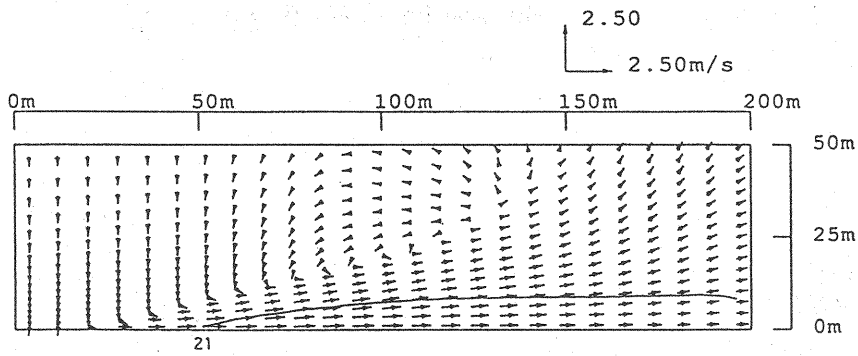


(a) plane view near free surface (k=14)

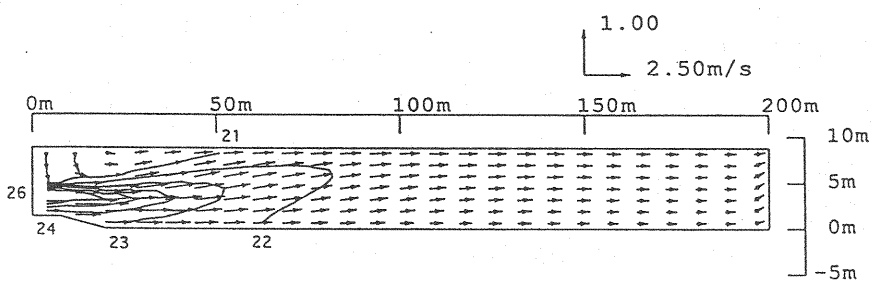


(b) vertical view along center line (j=1)

Fig. 2 Distribution of temperature and velocity vectors in initial conditions for CASE-A (unit of number = $°C$, line interval = 1 $°C$)

As a result of the computation for CASE-A, the constant maximum depth, 3.04m below the initial sand bed level, is obtained in 350 days. Fig. 3 shows the predicted velocity vectors, temperature distribution and generated coordinates with the steady bed profiles. In this steady state, bottom shear stress is less than the critical value and the sediment concentration is zero in all area.

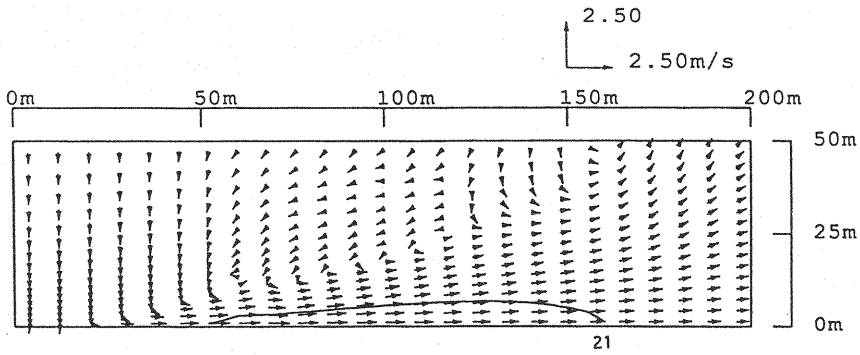


(a) plane view near free surface (k=14)

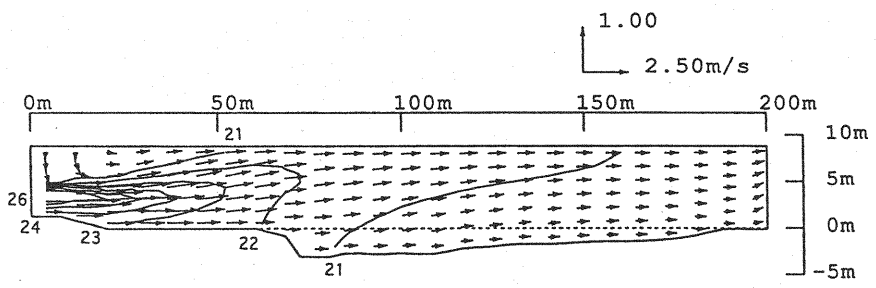


(b) vertical view along center line (j=1)

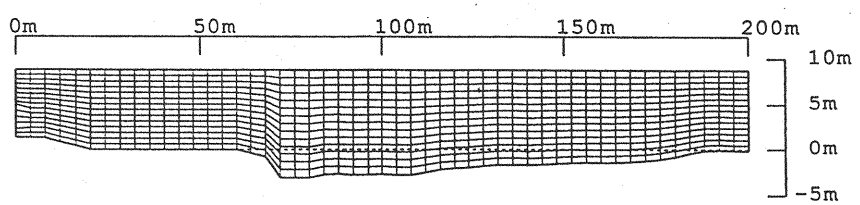


(c) vertical view along center line (j=1)

Fig. 3 Distributions of temperature, velocity vectors and generated mesh in final steady state for CASE-A (unit of number = $°C$, line interval = 1 $°C$)

The prediction for CASE-B is started with the final bed profiles in CASE-A and additional discharge from the upstream boundary. The initial steady flow field, shown in Fig. 4, is first calculated by setting the bed profiles are not changed by the increased discharge.

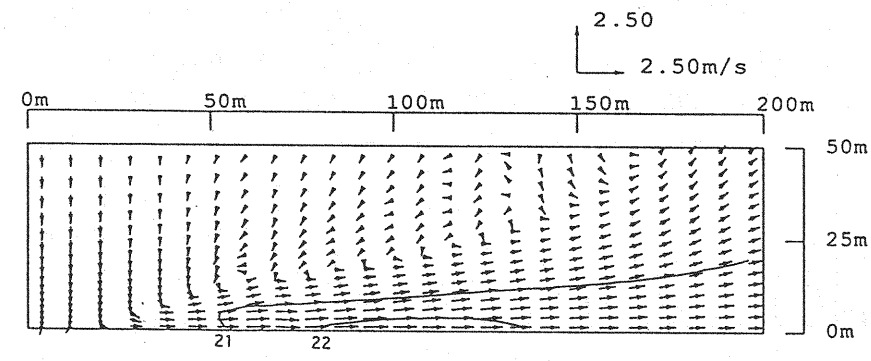


(a) plane view near free surface (k=14)

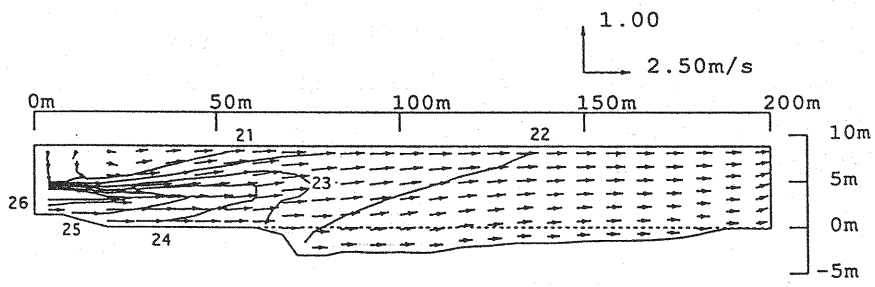


(b) vertical view along center line (j=1)

Fig. 4 Distribution of temperature and velocity vectors in initial conditions for CASE-B (unit of number = $°C$, line interval = 1 $°C$)

Since the flow rate is doubled in CASE-B, the high temperature fluid is extended downward and near-surface regions compared with the results in Fig. 2. After about 400 days from additional discharge, the maximum depth becomes constant, 4.56m below the initial level. Fig. 5 shows the velocity vectors, temperature distribution and generated mesh obtained on steady bed profiles in CASE-B.

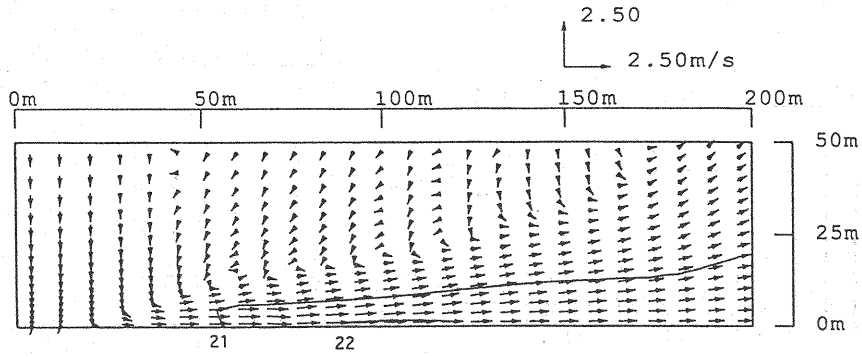


(a) plane view near free surface (k=14)

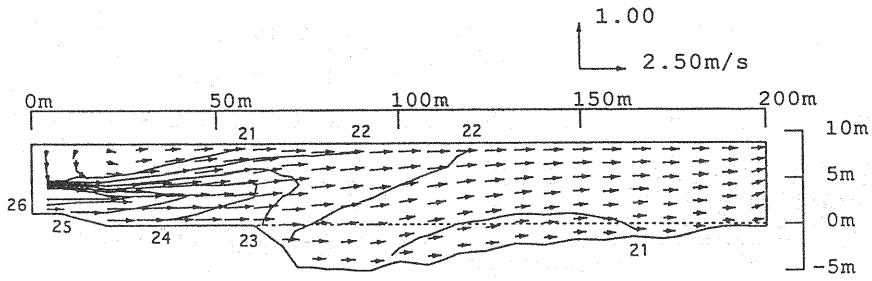


(b) vertical view along center line (j=1)

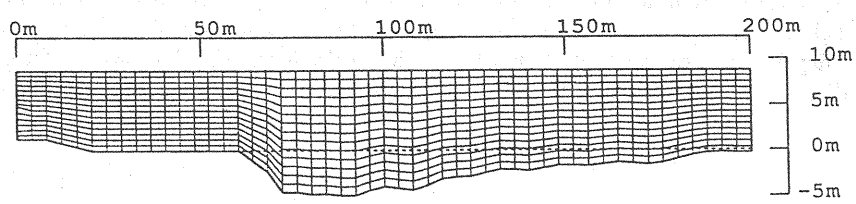


(c) vertical view along center line (j=1)

Fig. 5 Distributions of temperature, velocity vectors and generated mesh in final steady state for CASE-B (unit of number = $°C$, line interval = 1 $°C$)

The contour maps for bed profiles are shown in Fig. 6. While the predicted width of the scoured area is somewhat narrower than that of the measured results, the fact that the deeply scoured positions appear on the center line just downstream the SPAC region is predicted in the calculated results. The difference in the width of the scoured area might be caused by the meandering of the discharged flows due to nearshore currents in the actual field, which are not taken into account in the numerical model.

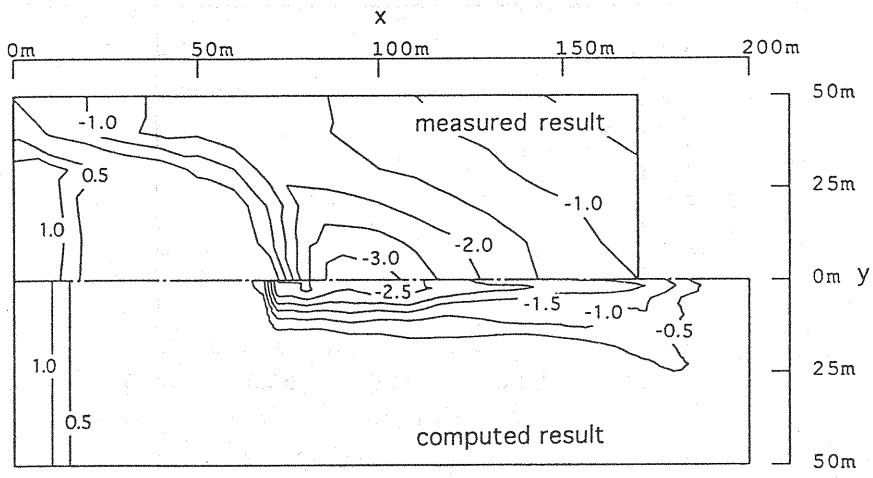


(a) CASE-A

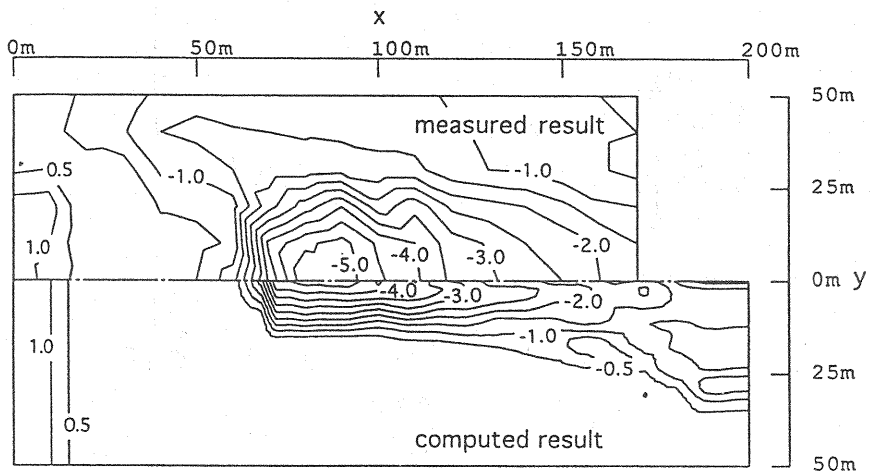


(b) CASE-B

Fig. 6 Contour maps for scoured sand bed profiles (number $= z+1.3m$, line interval $= 1\ m$)

The comparison of the bed profiles on the center line, including the deeply scoured area, is presented in Fig. 7. It can be seen that the measured bed profiles both in CASE-A and B are in reasonable agreement with the predicted results.

## CONCLUDING REMARKS

A numerical prediction method has been developed for bed deformation due to three-dimensional turbulent flows affected by buoyancy force. In this method, the buoyant flows and sediment transportation are predicted with a two-equation turbulence model. The effects of the unsteadily deformed bed profiles on a flow field are adequately taken into account, since the boundary shapes are precisely represented using three-dimensional boundary-fitted coordinates, which are regenerated to respond to unsteady deformation. In this coordinate system, the moving boundary is treated with the ALE formulation and the governing equations are transformed into computational space, where discretization is made with sufficient numerical accuracy.

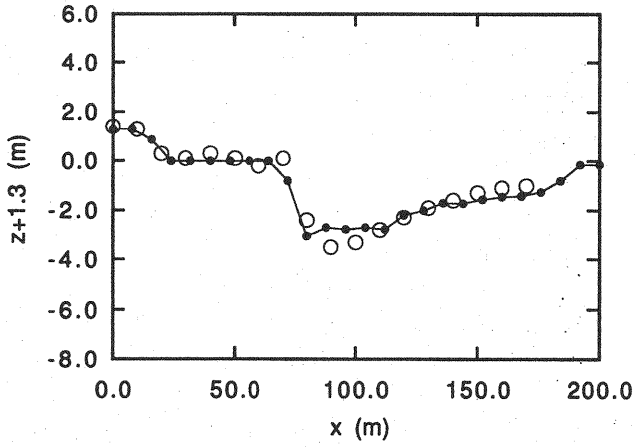


(a) CASE-A

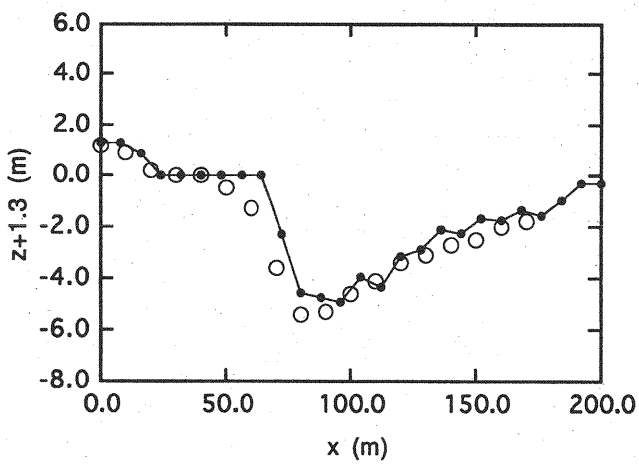


(b) CASE-B

Fig. 7 Sand bed profiles on center line (○=measured, ●=predicted)

This computational method was applied to the results of the field measurements in front of a power station. As a result, while the predicted width of the scoured area is narrower than that of the measured results, it is shown that the bed profiles on the center line, including the most scoured area, are reasonably predicted both in two different discharge conditions. In terms of the accuracy and the generality of the present numerical model and solution algorithm, this computational method is expected to be applied to wide range of sediment transportation and bed-deformation problems in hydraulics.

## REFERENCES


1. Ushijima, S., Shimizu, T., Sasaki, A. and Takizawa, Y. : Prediction method for local scour by warmed cooling-water jets, ASCE Journal of Hydraulics Engineering, Vol.118, No.8, pp.1164 1183, 1992.

2. Olsen, N. R. B. and Melaaen, M. C. : Three dimensional calculation of scour around cylinders, ASCE Journal of Hydraulics Engineering, Vol.119, No.9, 1993.

3. Ushijima, S. : Arbitrary Lagrangian-Eulerian numerical prediction for local scour caused by turbulent flows, J. Comp. Phys., vol.125, No.1, 71-82, 1996.

4. J. F., Warsi, Z. U. A. Thompson and Mastin, C. W. : Numerical Grid Generatio, Elsevier, New York, 1985.

5. Hirt, C. W., Amsden, A. A., and Cook, J. L. : An arbitrary Lagrangian-Eulerian computing method for all flow speeds, J. Comp. Phys., vol.14, 227-253, 1974.

6. Ushijima, S. : Prediction of thermal stratification in a curved duct with 3D boundary-fitted coordinates, International Journal for Numerical Methods in Fluids, Vol.19, pp.647-665, 1994.

7. Ushijima, S., Moriya, S., Tanaka, N. : Internal standing waves in a cylindrical vessel, and their near-wall features, ASME, J. Heat Transfer, Vol.115, 613-620, 1993.

8. Launder, B. E. : On the effects of a gravitational field on the turbulent transport of heat and momentum, J. Fluid Mech., Vol. 67., 1975.

9. Rodi, W. : Turbulence models, their application in hydraulics, A state of the art review presented by the IAHR section on fundamentals of division II experimental, and mathematical fluid dynamics, 1980.

10. Harlow, F. H. and Welch, J. E. : Numerical calculation of time-dependent viscous incompressible flow of fluid with free surface, Phys. Fluids 8, 2182-2189, 1965.

11. Nakagawa, H. and Tsujimoto, T. : Sand bed instability due to bed load motion, Proc. ASCE, J. Hydr. Div., ASCE, 106(12), 2029-2051, 1980.

12. Jonsson, I. G. : Wave boundary layers and friction factors, Proc. 10th Conf. on Coastal Eng., 127-148, 1966.

13. Shimizu, T., Ikeno, M., Ujiie, H., Yamauchi, K. : Plane design of SPAC countermeasure against seabed scour due to submerged discharge, and large waves, Proc. 24th Int. Conf., Coastal Eng. Res. Council/ASCE, 3320-3334, 1994.

## APPENDIX-NOTATION

*The following symbols are used in this paper:*

| | |
|---|---|
| $B$ | = sand bed height; |
| $C$ | = sand concentration; |
| $C_k, C_\nu, C_\epsilon, C_{\epsilon 1}, C_{\epsilon 2}$ | = coefficients of turbulence model; |
| $d$ | = diameter of sand particle; |
| $g$ | = gravity; |
| $g_i$ | = $x_i$ component of gravity force; |
| $k$ | = turbulence energy; |
| $P_m$ | = contral function; |
| $P_{rt}$ | = turbulent Prandtl number; |
| $p$ | = mean pressure; |
| $p_s$ | = pick-up rate; |
| $q_i$ | = sand flux in $x_i$ direction; |
| $T$ | = mean temperature; |
| $t$ | = time in physical space; |
| $U_{0m}$ | = contravariant grid velocity component; |
| $U_m$ | = contravariant velocity component; |
| $u_i$ | = mean velocity component in $x_i$ direction; |
| $u_{i*}$ | = friction velocity in $x_i$ direction ($i = 1, 2$); |
| $w_0$ | = falling velocity of sand; |
| $x_i$ | = coordinates in physical space; |
| $\alpha$ | = thermal conductivity; |
| $\beta$ | = thermal expansion coefficient; |
| $\gamma$ | = porosity of bed material; |
| $\Delta T$ | = temperature difference from standard value; |
| $\Delta t$ | = time increment; |
| $\epsilon$ | = dissipation rate of turbulence energy; |
| $\epsilon_H$ | = eddy conductivity; |
| $\epsilon_M$ | = eddy viscosity; |
| $\epsilon_S$ | = turbulent diffusivity for $C$; |
| $\lambda$ | = molecular diffusivity for $C$; |
| $\nu$ | = kinematic viscosity; |
| $\xi_m$ | = coordinates in transformed space; |
| $\rho$ | = fluid density; |
| $\sigma$ | = density of sand particle; |
| $\tau$ | = time in transformed space; |
| $\tau_*$ | = normalized bottom shear stress; |
| $\tau_{*f}$ | = $\tau_*$ caused by flow; |
| $\tau_{*wm}$ | = $\tau_*$ caused by wave motion; |

(Received September 28, 1998 ; revised January 11, 1999)